Heliyon 9 (2023) e13030

Contents lists available at ScienceDirect

Heliyon

journal homepage: www.cell.com/heliyon

Research article

Predicting the essential oil composition in supercritical carbon dioxide extracts from hop pellets using mathematical modeling

Verena Bernadette Pannusch [a], Lukas Viebahn [b], Heiko Briesen [a], Mirjana Minceva [b,*]

[a] Process Systems Engineering, Technical University of Munich, Freising, Germany
[b] Biothermodynamics, Technical University of Munich, Freising, Germany

ARTICLE INFO

Keywords:
Monoterpene
Sesquiterpene
Pressure
Temperature
Beer
Aroma

ABSTRACT

Supercritical fluid extraction from hops (*Humulus lupulus* L.) can be used to extract essential oil for the flavoring of beer. With a special focus on the oil composition being linked to the hop aroma, the influence of pressure and temperature on the extraction kinetics of seven oil components (β-myrcene, α-humulene, β-caryophyllene, 2-methylbutyl isobutyrate, undecanone, linalool, and α-pinene) is analyzed and modeled in this article.

Supercritical CO_2 extraction from hop pellets was conducted at pressure-temperature combinations of 90/100/110 bar and 40/45/50 °C. The extract composition over time, analyzed by gas chromatography, was used for the parameterization of two existing mechanistic models: an internal-mass-transfer-control (IMTC), and a broken-and-intact-cells (BIC) model. The IMTC model was found to effectively describe most extraction kinetics and hence applied in this study. In contrast to previous studies, the IMTC model parameters were not only fitted to individual extraction curves from different experiments but also correlated to temperature and pressure as a further step towards model-based prediction. Using the parameterized model, the extract composition was predicted at 95 bar/48 °C, 105 bar/42 °C, and 105 bar/48 °C.

Extraction yields were found to be higher at lower temperatures and higher pressures in general. The sensitivity towards pressure was observed to differ between components and to be particularly higher for β-myrcene compared with α-humulene. Changes of the essential oil composition with a variation in pressure and temperature were predicted correctly by the model with a mean relative deviation from experimental data of 11.7% (min. 1.2%, max. 36.2%).

1. Introduction

Due to both economic and environmental advantages, more and more industries are transitioning to the use of supercritical carbon dioxide instead of organic solvents in extraction processes [1]. In addition to its GRAS status (Generally Recognized As Safe), supercritical carbon dioxide ($scCO_2$) also offers a couple of advantages with regard to the extraction process. Its low critical temperature of 31 °C enables extractions to be carried out in relatively mild conditions. Consequently, delicate solutes like odor-active essential oils are extracted without chemical alteration or thermal degradation [2]. Since CO_2 is gaseous in standard conditions, a drop in pressure and temperature in the collection vial suffices for an almost complete evaporation of the solvent, making additional purification steps for solvent removal unnecessary.

* Corresponding author.
E-mail address: mirjana.minceva@tum.de (M. Minceva).

https://doi.org/10.1016/j.heliyon.2023.e13030
Received 30 August 2022; Received in revised form 10 January 2023; Accepted 13 January 2023
Available online 18 January 2023

The common hop (*Humulus lupulus* L.) has been employed in the brewing industry for centuries [3]. While they are quantitatively a minor ingredient in the process, added at the wort boiling step, they have a large impact on the aroma, taste, foam, stability, and mouthfeel of beer [4–6]. Hop products impart bitterness and a wide range of flavors to beer, including fruity, resinous, herbal, tropical, or citrus-like aroma impressions [7].

The two primary value-adding components of dried hop cones are soft resins (10–25%) and essential oils (0.4–2%). The main soft resins are α- and β-acids which impart bitterness and have a strong antimicrobial effect. The volatile essential oils comprise terpenes, sesquiterpenes and their respective oxygenated derivatives, esters, ketones as well as thiols. Some of them are highly odor-active and are responsible for the characteristic aroma of hops [8–10].

The research field of supercritical fluid extraction (SFE) of essential oil is replete with groups investigating a large number of plants and target molecules [11–14]. Recent studies shift the emphasis from the goal of maximum overall yield towards selective fractionation of the extract, e.g., by step-wise temperature [15] or pressure reduction [16]. Higher concentrations of bio-active target molecules in the fractions could be achieved by adjustment of temperature and pressure conditions in the separators [15,16]. With regard to hop cones, SFE is commonly used to produce extracts for beer hopping. Typical pressures lie between 300 and 500 bar, and temperatures range between 50 and 60 °C [17], targeting maximum yield of both bitter acids and aroma compounds. To achieve higher concentrations of aroma molecules in the extract, a more sophisticated selection of pressure and temperature is needed utilizing the specific solubility of essential oil components. Previous researchers have investigated using $scCO_2$ in novel analytical methods for hop volatiles [18,19] or the selective recovery of hop aromas for beer flavoring [20]. Nagybákay et al. [21] attempted to optimize the extraction of lipophilic antioxidants from hops.

With regard to the mathematical modeling of essential oil extraction from hops, a recent study by Bizaj et al. [22] applied a simple mathematical model to describe the extraction kinetics of total hop extract using various solvents. Kupski et al. [23] compared three different models to describe the total extract mass as a function of time with regard to $scCO_2$ extraction from ground hop. The authors found that the broken-and-intact-cells (BIC) model by Sovová [24] yielded the best fit for ground hops, one which has been successfully applied to many herbaceous raw materials like pennyroyal leaves [25], rosemary leaves [26], guava leaves [27], and many others. However, one drawback of the BIC model is the larger number of parameters to be fitted compared to other approaches, such as the internal-mass-transfer-control (IMTC) model [28]. The research presented here compares the latter two models, considering the goodness-of-fit of the models as well as their simplicity, i.e., the number of parameters to be fitted.

Former studies predominantly focused on total or essential oil yield. Considering the essential oil composition, i.e., the individual extraction kinetics of molecules, may, however, be beneficial for process design in order to enhance the extract quality and to selectively extract certain desired compounds with higher purity. Furthermore, a variety of models have accurately described $scCO_2$ extraction kinetics, but their potential for prediction and process optimization by including temperature and pressure correlations and considering the density of CO_2 in the model equations has still not been exploited.

With craft beer being globally on the rise, the demand for strong hop flavors in beer has changed the brewing industry worldwide. The focus is no longer on high α-acid utilization rates, but on a hoppy flavor achieved by "dry-hopping" procedures. Therefore, hops are not only added at the wort boiling step, but also at the end of the fermentation step and prior to the filling step at temperatures below 20 °C [29]. The subsequent separation of plant matter along with the non-isomerized α-acids inevitably results in losses of both bitter resins and beer. Technological advances will be required in order to reduce the waste of resources while increasing transfer rates of volatiles and resins. By separately extracting α-acids and essential oil using SFE with distinct operating conditions and adding them at different stages in the brewing process, both components can release their full potential while the waste of hop material is substantially reduced. For a targeted fractionation, however, the extraction behavior of the volatiles out of the complex hop matrix needs to be predictable.

The focus of this research is to investigate, model, and predict the extraction kinetics of individual essential oil components from hop pellets as functions of the operating parameters of temperature and pressure, i.e., solvent density. The results of this study may pave the way towards improved extract quality, higher yield, and less waste in the craft beer production, and in other applications of $scCO_2$ extraction from plant materials.

2. Material and methods

2.1. Materials

Hop samples (T90 pellets) from the 2020 Herkules crop were kindly supplied by Hopsteiner (Germany) in sealed vacuum packages

Table 1
List of chemicals, their purity specifications and producers.

Name	CAS Nr.	Purity, %	Supplier
β-Myrcene	123-35-3	91.8	Sigma-Aldrich (USA)
Linalool	78-70-6	98.8	Merck (Germany)
Undecanone	112-12-9	99.9	Acros Organics™ (USA)
L-Menthol	2216-51-5	99.6	Sigma-Aldrich (USA)
Ethanol abs.	64-17-5	99.98	VWR International (France)
Methyl-tert-butylether (MTBE)	1634-04-4	99.6	VWR International (France)
CO_2	124-38-9	99.7	Westfalen (Germany)

of 50.0 g. The composition as specified by the supplier is listed in Supplementary Information (SI) Table S1 online. The hop pellets had a mean density ρ_{hop} of 0.975 g cm^{-3} and were kept refrigerated until use.

All chemical substances used in this study, including their purity and supplier, are listed in Table 1.

2.2. Experimental methods

2.2.1. Supercritical fluid extraction

The extraction was carried out using an Applied Separations (USA) Spe-ed SFE Zoran extractor. The cylindrical extraction vessel has a volume of 100 mL, a length of 14.5 cm and an internal diameter of 3.0 cm. The vessel was charged by loosely filling it with 50.0 g of hop pellets and with glass wool at both ends acting as filter material. This reduced the effective bed length to 10.5 cm, resulting in a bed volume of 74 mL and a bulk density of 0.67 g cm^{-3}. The vessel was subsequently sealed, heated to the desired temperature, and filled with liquid CO_2. The pressure was then adjusted by the pump and the timer was started. The outlet valve was opened and the flow adjusted to 7 standard liters per minute (SLPM) (which is equal to a constant mass flow of 0.211 g s^{-1}) using the micro metering valve. The flow speed was measured at atmospheric pressure by an ALICAT Scientific (USA) digital flow meter and automatically corrected to 25 °C, 1.013 bar (SATP). 60 mL glass EPA vials were precooled to −27 °C in a freezer before being connected to the extractor and then cooled continuously in order to condensate any substances that might be volatile at room temperature. Samples were taken at 15 min intervals (9 samples per extraction) and all extractions were conducted in duplicates yielding 18 samples per experiment. The collected hop extract was stored at −27 °C. A flow chart of the process is shown in Fig. 1.

For analysis, the hop extract was dissolved in 10 mL of 70 vol% ethanol and 0.5 g of NaCl per 0.5 g of extract using an ultrasonic bath. The resulting extract solution was filtered using MACHEREY-NAGEL (Germany) Chromafil® PET-20/15 MS filters with a 0.20 μm pore size. The solution was kept at −27 °C in sealed tubes until further use.

2.2.2. Gas chromatography

All samples from time-resolved extract collection were analyzed via GC-FID. The hop volatiles in each extract sample were quantified by gas chromatography (GC) using a SHIMADZU (Japan) Nexis GC-2030 with flame ionization detector (FID). A SHIMADZU AOC-20i auto injector and a SHIMADZU AOC-20s Plus auto sampler were used for direct injection. The GC was equipped with a split-splitless injector which was held at 250 °C. The installed column was a Phenomenex® (USA) Zebron™ ZB5ms column (30 m length x 0.25 mm ID x 0.25 μm film thickness). A SHIMADZU P/N 221-75193 95 mm (deactivated, with wool) 3.4 mm ID liner was used. A carrier gas (helium) flow of 1.43 mL min^{-1} was maintained. The FID sampling rate was set to 40 ms and used a H_2 flow of 32 mL min^{-1} alongside a makeup flow (N_2) of 24 mL min^{-1} and an air flow of 200 mL min^{-1}. The chromatograms were analyzed using SHIMADZU LabSolutions™ software.

The samples consisted of 900 μL of filtered hop extract solution and 100 μL of menthol solution (5 mg l^{-1} dissolved in ethanol) as an internal standard (STD) whose peak does not overlap with the peaks of the characteristic essential oil components. The injected amount was 1 μL (single injection) and the split ratio was set to 1:50. The initial column temperature of 60 °C was held for 4 min before being raised to 280 °C at a rate of 10 °C min^{-1}. The final temperature was maintained for 3 min and the total time of analysis was 30 min. The FID temperature was set to 280 °C.

Given the complex nature of hop extract and possible matrix effects, STD addition was chosen as the calibration method [30]. Pure compounds of β-myrcene, linalool, and undecanone were added to a solution of commercial CO_2 hop extract provided by Hopsteiner (Germany). Additionally, each sample was spiked with an internal standard (menthol) in order to detect inconsistencies over the course of the measurements. A representative chromatogram is presented in Supplementary Fig. S37.

2.2.3. Solid density and total porosity

To determine pellet density, the mass of one pellet was measured using a precision scale. The diameter and length of the same pellet

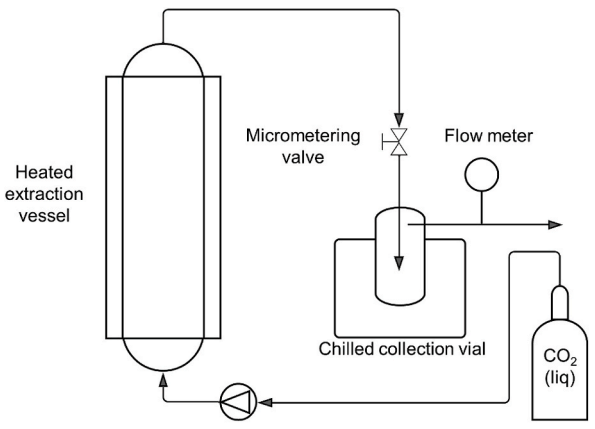

Fig. 1. Flow chart of scCO$_2$ extractor, Spe-ed SFE Zoran model (Applied Separations).

was measured using a caliper gauge and the cylinder volume determined. The mean pellet density ρ_{pellet} from 22 measurements was then calculated as:

$$\rho_{pellet} = \frac{1}{n_{pellet}} \sum_{i=1}^{n_{pellet}} \frac{m_{pellet,i}}{V_{pellet,i}} \tag{1}$$

with n_{pellet} being the number of measurements, $m_{pellet,i}$ being the mass of each pellet, and $V_{pellet,i}$ being the volume of the same pellet. The solid density ρ_s was measured in triplicate by helium pycnometry using a Micromeritics (Germany) AccuPyc 1330 pycnometer with a 10 cm^3 cylindrical measuring chamber. The inner porosity of the pellet ε_{pellet} was calculated from ρ_{pellet} (Equation (1)) as:

$$\varepsilon_{pellet} = 1 - \frac{\rho_{pellet}}{\rho_s} \tag{2}$$

The bulk porosity ε_{bulk} in the extraction column (without inner porosity ε_{pellet} of the pellets, Equation (2)) was calculated from the bulk density (mass of pellets per occupied column volume) and the pellet density as:

$$\varepsilon_{bulk} = 1 - \frac{m_0}{\frac{\pi}{4} d_i^2 L \rho_{pellet}} \tag{3}$$

with $_{m0}$ being the initial mass of hop pellets, L being the length of the extraction column, and d_i being the inner diameter of the extraction column. The total porosity ε describes the sum of the inner porosity and bulk porosity (Equation (3)):

$$\varepsilon = \varepsilon_{bulk} + (1 - \varepsilon_{bulk})\, \varepsilon_{pellet} \tag{4}$$

The inner porosity of the pellet ε_{pellet} (Equation (2)) was analyzed both before and after 135 min of extraction at 90 bar and 45 °C in order to investigate if and to which extent a change in porosity occurred. The results are shown in the Appendix.

2.3. Mathematical modeling

The mechanistic models used in this research describe the extraction of essential oil components from a packed bed of porous pellets using supercritical CO_2 as a solvent flowing through the pores of the cylindrical packed bed. During the extraction process, species dissolve, desorb, and diffuse from the inside of the leave fractions of which the pellets consist and to the surface, where they pass through a stagnant film to the flowing fluid in the pores. The extracted mass is then transported in the direction of CO_2 flow by forced advection and collected behind the column outlet, where it is separated from the solvent by expansion and vaporization of the solvent. Fig. 2 illustrates this modeling concept and presents three different scales. On the left, the sketched column is filled with the cylindrical pellets of equal radius, with CO_2 flowing in an upward direction. In the center circle, a representative volume element can be seen, with the solid leave fragments representing the solid phase of the porous pellets. The boxes on the right side of Fig. 2 show single particles and mass transfer by diffusion for the two models compared in this article: an internal-mass-transfer-control model (IMTC model) [28], and a broken-and-intact-cells model (BIC model) [31]. For the sake of readability, we will present the main equations of both models in the following sections. Please note that, in some cases, the notation may depart slightly from the original publications in order to better compare the two models used in this research. The interested reader is referred to the original publications for a more detailed derivation.

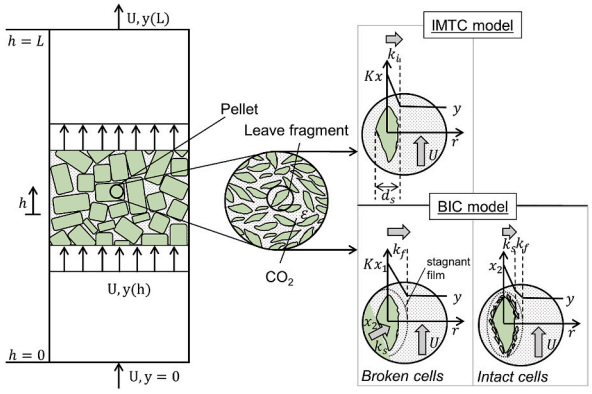

Fig. 2. Schematic illustration of the internal-mass-transfer-control model (IMTC) [28] and the broken-and-intact-cells model (BIC) [31]. Three different scales: the macroscale of the extractor column (left), a representative volume element (center), and a single leave fragment (right) with slab thickness d_s. Advection of fluid mass fraction y occurs in the direction of h along the column length L and with superficial velocity U. Mass transfer from leave fragments with solid mass fraction x is controlled by the partition coefficient K and by the internal mass transfer coefficient k_i (IMTC model) or by fluid-phase mass transfer coefficient k_f for broken cells, and by solid-phase mass transfer coefficient k_s for intact cells (BIC model). r represents the distance from the particle center.

In general, we made the following assumptions: (i) the fluid fully penetrates the pellets homogeneously, i.e., advection happens both between and inside pellets; (ii) the initial penetration and imbibition process, when CO_2 enters the extractor, displaces air, and fills the pores, is disregarded, so the porous medium is assumed to be filled with CO_2 at t = 0; (iii) structural parameters such as porosity and specific surface area (Equation (8)) remain constant; (iv) the temperature and pressure within the packed bed are constant in terms of both time and space, and (v) density and viscosity of pure CO_2 are assumed to be unaffected by the concentration of the solutes.

2.3.1. IMTC model

The IMTC model is based on the one-dimensional general diffusion model [32], with the assumption that internal mass transfer limits the extraction rate throughout the entire extraction process. This means that the external mass transfer is disregarded, and the concentration at the surface of a leaf fragment, which is modeled as a cuboid shaped slab, is expected to be the same as in the fluid bulk phase [28]. Fig. 2, at right, illustrates this assumption. The dominance of internal over external mass transfer resistance has been suggested as an appropriate assumption for extraction from leaves [33]. The IMTC model consists of the mass balance in the fluid phase:

$$\rho_f \, \varepsilon \left(\frac{\partial y}{\partial t} + U \, \frac{\partial y}{\partial h} \right) = j \tag{5}$$

and the mass balance in the solid phase:

$$\rho_s \, (1 - \varepsilon) \, \frac{\partial x}{\partial t} = - j \tag{6}$$

where x is the mass fraction of a species in the solid phase, y is the mass fraction of a species in the fluid phase, h is the spatial coordinate pointing upward in the direction of flow, t is the time, ρ_f is the fluid density, ρ_s is the solid density, ε is the total porosity of the packed bed of pellets (see Equation (4)), U is the superficial velocity, and j is the flux between fluid and solid phase. The volume averaged flux from the solid phase to the fluid phase neglecting external mass transfer is described by:

$$j = \rho_f \, k_i \, a \, (Kx - y) \tag{7}$$

where k_i is the internal mass transfer coefficient, a is the specific surface area of the solid phase, being:

$$a = \frac{2}{d_s} \, (1 - \varepsilon) \tag{8}$$

with slab thickness assumed to be $d_s = 21 \, \mu m$ [23] and K is the partition coefficient of a species:

$$K = \frac{y^*}{x} \tag{9}$$

The mass fraction in the fluid at equilibrium is represented by y^*. Based on the finding that plant tissue of hops swells and pores are hence filled with CO_2 [34], mass transport inside the leave fragments (thin slabs) is modeled as molecular diffusion in the intra-particle pore space. Accordingly, the driving force is the difference between the average solute concentration in the pore space of the leave fragments being y* and its concentration on the surface (equal to bulk concentration). Axial dispersion is disregarded (the relevant contributions are presented in the Supplementary Information, Equations (S.1) to (S.3), available online).

The initial conditions for a solute mass fraction in the fluid and solid phase, respectively, are:

$$y|_{t=0} = 0 \, ; \quad x|_{t=0} = x_0 \tag{10}$$

where x_0 is the initial solute mass fraction in the solid phase. Please note that we assume the initial concentration in the fluid phase to be zero, i.e., the pore space is filled with pure $scCO_2$. The boundary condition at the inlet of the extractor is defined by:

$$y|_{h=0} = 0 \tag{11}$$

The cumulated extracted solute mass E in the CO_2 extract is obtained by:

$$E = \rho_{f,out} \, Q_{CO_2} \int_0^t y|_{h=L} \, dt' \tag{12}$$

where Q_{CO_2} is the volume flow of CO_2, $\rho_{f,out}$ is the fluid density at the outlet pressure of 1 bar (after expansion) and a temperature of 20 °C. The respective yield Y is:

$$Y = \frac{E}{m_0} \tag{13}$$

with m_0 being the total mass of hop pellets at the beginning of extraction ($t = 0$).

The above model has been transformed into dimensionless form and normalized for numerical solution, which is shown in the Supplementary Information online (Equations (S.4) to (S.9)).

2.3.2. BIC model

With regard to the BIC model, it is expected that two extraction stages exist, the former being controlled by the solution equilibrium of a solute in CO_2 (see Equation (9)) due to quick fluid-phase (external) mass transfer from broken cells, and the latter being limited by the solid-phase (internal) mass transfer resistance in intact cells [31]. In contrast with the IMTC model, it is in this case assumed that, in addition to intact cells with internal mass transfer control, a second solid phase of broken cells also exists at the surface of intact cells which is controlled by external mass transfer only. As a result, diffusion occurs from intact cells to broken cells and from broken cells into the fluid. The two sketches at the lower right of Fig. 2 illustrate these relations.

The BIC model equations by Sovová [31] consist of the mass balance of solutes in the fluid phase:

$$\rho_f \, \varepsilon \left(\frac{\partial y}{\partial t} + U \, \frac{\partial y}{\partial h} \right) = j_f \tag{14}$$

the mass balance in broken cells:

$$r \, \rho_s \, (1-\varepsilon) \frac{\partial x_1}{\partial t} = j_s - j_f \tag{15}$$

and the mass balance in intact cells:

$$(1-r) \, \rho_s \, (1-\varepsilon) \frac{\partial x_2}{\partial t} = -j_s \tag{16}$$

In the above model, there are two fluxes, j_f describing the flux from the broken cells to the fluid and j_s being the flux from the intact cells to the broken cells. The mass fraction of a species in broken cells is represented by x_1, the mass fraction in intact cells is x_2.

Parameter r stands for the volume fraction of broken cells. The flux from broken cells to the fluid is described by:

$$j_f = k_f \, a \, \rho_f \, \left(y^* - y \right) = k_f \, a \, \rho_f \, \left(K \, x_1 - y \right) \tag{17}$$

where k_f represents the fluid-phase mass transfer coefficient and the flux from the intact cells to the broken cells is:

$$j_s = k_s \, a \, \rho_s \, (x_2 - x_1) \tag{18}$$

with k_s being the solid-phase mass transfer coefficient.

The initial and boundary conditions for this set of partial differential equations are:

$$y|_{t=0} = y_0 \; ; \quad x_1|_{t=0} = x_{1,0} \; ; \quad x_2|_{t=0} = x_{2,0} \; ; \quad y|_{h=0} = 0 \tag{19}$$

The initial mass fraction in the broken cells is $x_{1,0}$ and the initial mass fraction in the intact cells is $x_{2,0}$. The extracted mass of a solute at time t is calculated by Equation (12), similar to the IMTC model.

Regarding the fluxes j_f and j_s, Sovová [31] proposes different terms, depending on the initial concentration of a solute. A type D extraction (Sovová's classification: initial equilibrium below saturation concentration), suitable for essential oil extraction from leaves and flowers, was selected in this case as the initial condition for the fluid phase:

$$y_0 = y^* \left(x_{1,0} \right) = K \, x_{1,0} \tag{20}$$

The type D equilibrium was selected based on the shape of extraction curves observed in this study (smooth transition between stages) and on the fact that the operational solubility determined from the initial slope was lower than the theoretical solubility of essential oil components [35,36]. The initial amount of free solute in the broken and intact cells is described by:

$$x_{1,0} = \frac{r \, x_u}{r + \gamma \, K} \; ; \quad x_{2,0} = x_u \tag{21}$$

The parameter x_u defines the mass fraction of a species in the insoluble solid and γ is:

$$\gamma = \frac{\rho_f \, \varepsilon}{\rho_s \, (1-\varepsilon)} \tag{22}$$

The model equations are transformed into dimensionless form as described in Ref. [31].

2.4. Numerical solution and parameter fitting

All computations were performed on a computer with the following specifications: Intel(R) Core(TM) i7-8700 CPU @ 3.20 GHz, 3.19 GHz, 16.0 GB RAM memory, equipped with a NVIDIA GeForce GT 1030 graphic card and a Microsoft Windows 10 Enterprise operating system.

The systems of partial differential equations for both models were solved numerically using finite differences. A five-point biased upwind scheme was used for the spatial coordinate [37]. The solution of the resulting ordinary differential equations and algebraic equations was implemented in MATLAB® R2020b (MathWorks, Massachusetts, USA) using the "ode15s" function.

For parameter fitting, the non-linear least squares solver "lsqnonlin" and the linear fit solver "robustfit" were used, and the sum of

squared residuals between the experimental and simulated cumulated mass of extract (Equation (12)) was minimized. The fitting procedure applied in this research for achieving predictions of extraction kinetics as a function of extraction temperature and pressure is divided into four steps: I) fitting model parameters to data from single extraction experiments; II) model selection; III) correlations of model parameters with temperature and pressure; IV) fitting correlation parameters to all experimental data using fitted parameters from step 3 partially as starting values for the numerical iterations and partially as constants.

2.4.1. Fitting model parameters to single experiments

Regarding the IMTC model, three unknown model parameters were fitted: $k_i a$, $y^*(x_0)$, and x_0. In order to more closely approach a global minimum, three start values for $k_i a$ were investigated: 0.01, 0.001, and 0.0001. The goodness-of-fit was evaluated by the mean absolute percentage error (MAPE, %):

$$MAPE = \frac{1}{n}\sum_{i=1}^{n} abs\left(\frac{E_{i,exp} - E_{i,sim}}{E_{i,exp}}\right) * 100 \tag{23}$$

The combinations of parameters exhibiting the lowest MAPE were selected and used for the subsequent fitting steps.

As for the BIC model, the procedure presented in Ref. [31] was applied. The unknown parameters in this model to be fitted are $y^*(x_{1,0})$, r, $k_s a$, $k_f a$. The initial solid-phase mass fraction necessary for this model (Equation (21) and (22)) was determined by either using the supplier's information (see SI Table S1 online), or, if no data was available, the maximum yield from experiments. The respective data are included in SI Table S2 online. In a first step, the operational solubility (initial outlet concentration in case of equilibrium conditions and free solute, Equation (20)) was determined by defining the initial slope of the extraction curve from the derivative of a fitted 6th degree polynomial at $t = 0$. Start values for r and $k_s a$, as well as the value of K were calculated as described in Ref. [31]. A reasonable initial guess for k_f was determined from a correlation found in the literature (by Puiggené et al. [38]), which defines the Sherwood number:

$$Sh = 0.206\, Re^{0.80} Sc^{1/3} \tag{24}$$

where Re is the particle Reynolds number and Sc is the Schmidt number. This yields the fluid-phase mass transfer coefficient:

$$k_f = \frac{Sh\, D_{12}}{d_s} \tag{25}$$

with D_{12} being the binary diffusion coefficient of the respective essential oil compound. $D_{12}(p, T)$ was approximated by using the correlation by Catchpole and King [39]. The density and viscosity of supercritical CO_2 for the respective temperature and pressure, which are necessary to calculate Re, Sh (Equation (24)), and k_f (Equation (25)), were calculated from thermodynamic correlations [40, 41].

After all of the start values were determined, r was fitted to all experimental data, individually for each substance. Although it might be assumed that r is not substance-specific, fitting r to all substance data at once yielded unsatisfactory results. The resulting value of r was subsequently taken as a constant, and the parameters $k_s a$ and $k_f a$ were fitted to each individual experimental run.

2.4.2. Model selection

The IMTC model and the BIC model were compared using a modified Akaike criterion (AIC_c) for sample numbers less than 40 [42]:

$$AIC_c = n\left[\ln\left(\frac{RSS}{n}\right)\right] + 2g + \frac{2g(g+1)}{n-g-1} \tag{26}$$

In this case, n is the number of samples, RSS is the residual sum of squares, and g is the number of fitted parameters which is three for the IMTC model ($k_i a$, $y^*(x_0)$, and x_0) and four in the BIC model ($k_f a$, $k_s a$, $y^*(x_{1,0})$, and r). The model identified as preferable at most conditions was selected for further use in order to cover the range of temperature and pressure conditions.

2.4.3. Correlations of model parameters with temperature and pressure

The correlation equations used to describe the model parameters (fitted in step I) for the selected model as functions of temperature and pressure are presented in the following. The three correlation equations with fitting parameters, specified as $\boldsymbol{\alpha}$, $\boldsymbol{\beta}$, and $\boldsymbol{\gamma}$, were fitted to the model parameters obtained in fitting step (I). Vectors of fitting parameters are subsequently highlighted in bold.

With regard to the equilibrium concentration $y^*(x_0)$ in supercritical CO_2, a correlation equation by Chrastil [43] was used which is based on the reaction kinetics of the solvato complex formation between a molecule and a gas and is defined by:

$$c^*(p,T) = \rho_f(p,T)^{\boldsymbol{\alpha}_1}\ e^{\left(\frac{\boldsymbol{\alpha}_2}{T} + \boldsymbol{\alpha}_3\right)} \tag{27}$$

In this case, the fitting parameters are α_1, α_2, and α_3; p and T are the extraction pressure in MPa and temperature in Kelvin, c^* is the equilibrium concentration in g dm^{-3}, and ρ_f is the fluid density in g dm^{-3}. The relation between volume-based equilibrium concentration c^* (mass per volume CO_2) and mass fraction y^* (mass per mass CO_2) is given by:

$$y^*(p,T) = \frac{c^*(p,T)}{\rho_f(p,T)} \tag{28}$$

Temperature is directly included in Equation (27), whereas the influence of pressure is included in its impact on the fluid density. The pressure and temperature function of CO_2 density is received from Ref. [40].

According to Ref. [44], the internal mass transfer coefficient k_i is related to the effective diffusion coefficient D_e in the solid phase by:

$$D_e(p,T) = \frac{k_i\, d_s}{6\,(1-\varepsilon)} \tag{29}$$

which is furthermore related to the binary diffusion coefficient of a species by:

$$F_M(p,T) = \frac{D_{12}(p,T)}{D_e(p,T)} \tag{30}$$

with F_M being a microstructural factor which includes diffusion hindrance as well as interactions with the solid matrix. A correlation of D_{12} for each substance with pressure and temperature was determined using a method by Catchpole and King [39]. To account for changes of F_M with pressure and temperature, a second-order model was used:

$$F_M(p,T) = \beta_1 + \beta_2 p + \beta_3 T + \beta_4 p^2 + \beta_5 T^2 + \beta_6 pT \tag{31}$$

Six fitting parameters are required, represented by the vector $\boldsymbol{\beta}$. The above type of correlation, with up to second order expressions, is commonly used for the description of response surfaces from two factors.

The initial mass fraction x_0 was also found to change with pressure and temperature. The dependence of x_0 on the latter variables is as well described by a second-order model applying to all components except α-pinene:

$$x_0(p,T) = \gamma_1 + \gamma_2 p + \gamma_3 T + \gamma_4 p^2 + \gamma_5 T^2 + \gamma_6 pT \tag{32}$$

With respect to α-pinene, a first-order correlation of the type:

$$x_0(p,T) = \gamma_1 + \gamma_2 p + \gamma_3 T \tag{33}$$

was applied because a second-order correlation would have over-estimated curvature and yielded negative values in the area of small concentrations without significantly improving the goodness-of-fit.

2.4.4. Fitting correlation parameters to all experiments

In the last fitting step, the correlation vectors $\boldsymbol{\beta}$, and $\boldsymbol{\gamma}$, fitted in step III were kept constant, and the vector $\boldsymbol{\alpha}$ describing the dependence of $y^*(x_0)$ on temperature and pressure was fitted to all 18 experiments (index i) , including all 9 sampling times (index j) for each of the essential oil components analyzed and for the total mass of extract. The regression problem is then:

$$\min_{\boldsymbol{\alpha}} \sum_{i=1}^{18} \sum_{j=1}^{9} \left(E\left(\boldsymbol{\alpha},\boldsymbol{\beta},\boldsymbol{\gamma},p_i,T_i,t_j\right) - E_{exp,i,j}\right)^2 \tag{34}$$

The fitted $\boldsymbol{\alpha}$ from step 3 was used as an initial guess.

3. Results and discussion

The results of this study will be presented in three sections: 1) selection of a model for the description of extraction kinetics; 2) study of the influence of pressure and temperature on the extraction kinetics, extract yield, and composition; and 3) prediction of the latter using the selected and parameterized model. Seven volatiles were investigated in the scope of this research: β-myrcene, α-humulene, β-caryophyllene, 2-methylbutyl isobutyrate (2-MBIB), undecanone, linalool, and α-pinene (in decreasing order of content). Additionally, the total mass of extract was assessed for the evaluation of yield and extract composition. For the sake of brevity, the parameter fitting results are shown subsequently for (a) β-myrcene as a representative monoterpene, (b) α-humulene as a representative sesquiterpene, and (c) total mass of extract. These three representative extraction curves are adequate for demonstrating both the development of extract composition and the overall yield. A full factorial design of experiments was applied with three settings each for extraction pressure and temperature: 90, 100, and 110 bar and 40, 45, and 50 °C.

3.1. Model selection and parameterization

The IMTC model (Equations (5) to (7)) with the initial and boundary conditions presented in Equations (10) and (11) and the BIC model (Equations (14) to (18)), with initial and boundary conditions described by Equation (19), were compared with respect to their goodness-of-fit and numbers of fitting parameters. Simulations of extraction yield, calculated by Equation (13), for both fitted models are depicted in Fig. 3 together with the experimental data. β-Myrcene, α-humulene, and total mass yield are shown at a representative condition of T = 40 °C and p = 100 bar which is equivalent to a density of about 629 kg m^{-3}. Plots of all other investigated pressure-

temperature combinations are presented in the Supplementary Information (SI) Figs. S1–S8 online. The experimentally derived value for total porosity ε is included in Appendix A.

Table 2 lists the respective fitted parameters of both models for T = 40 °C and p = 100 bar, as well as the MAPE (Equation (23)) and AIC_c (Equation (26)). The results for MAPE and AIC_c in all other analyzed experimental conditions and volatiles are available in SI Table S3 online. With respect to these conditions, it is evident that the values of MAPE and AIC_c for the IMTC fit are lower than those for the BIC fit. Particularly for β-myrcene, a lack of fit is visible when using the BIC model, as shown in Fig. 3. Although this is not the case in all experimental conditions (see SI Table S3 online), the mean AIC_c values across all experiments (shown in Table 3) are lower for the majority of components in the case of the IMTC model. This indicates that the IMTC model is superior to the BIC model for this process because it requires fewer parameters and leads to a comparable or even better fit. In addition to the foregoing argument, the fitted value of the BIC parameter r describing the volume fraction of broken cells varies for different substances, indicating a lack of identifiability, and is rather low, in particular for total mass, at 0.0149. This supports the assumption that the impact of a broken cells phase characterized by a high mass transfer rate is negligible for the system investigated. Consequently, the IMTC model was selected and subsequently used to correlate model parameters with temperature and pressure (respective fitted and experimental extraction curves at all operating conditions available in SI Figs. S9-S15 online). Although internal mass transfer has been shown to control SFE from hops in CFD simulations [45], the IMTC model has not yet been proposed for modeling SFE kinetics from hops [23]. According to the high goodness-of-fit achieved (MAPE <5%, presented in Table 2), the IMTC model may serve as a model of choice in the scope of essential oil extraction from hops.

3.2. Influence of pressure and temperature on extraction kinetics

The specific influence of extraction pressure and temperature on the essential oil profile is unknown *a priori*. Accordingly, relations of the kinetic model parameters as functions of pressure and temperature are required in order to predict extraction under different conditions. As a first step, the IMTC model was fitted to the single extraction curves. Based on the results, it was observed that all model parameters, i.e., $y^*(x_0)$, $k_i a$, and x_o changed with temperature and pressure. These relations to T and p can be described by the functions $c^*(\boldsymbol{\alpha}, p, T)$ (see Equation (27)), $F_M(\boldsymbol{\beta}, p, T)$ (see Equation (31)), and $x_0(\boldsymbol{\gamma}, p, T)$ (see Equations (32) and (33)), respectively. The parameters $\boldsymbol{\beta}$ (6 parameters) and $\boldsymbol{\gamma}$ (6 or 3 parameters in case of α-pinene) were each fitted to all 18 fitted model parameters (see Figs. 4 and 5). Thereupon, $\boldsymbol{\alpha}$ (3 parameters) was fitted to the extracted solute mass data $E(t)$ at all of the 9 pressure-temperature combinations investigated (162 data points in total; see Equation (34)), keeping $\boldsymbol{\beta}$ and $\boldsymbol{\gamma}$ constant.

The microstructural factor F_M, characteristic for the intraparticle diffusion hindrance, was calculated for each value of k_i and the parameter vector $\boldsymbol{\beta}$, correlating F_M to pressure and temperature, was fitted (see Equations (29)–(31)). A plot of the fitted model function $F_M(p, T)$ is shown in Fig. 4 together with the 18 data points it was fitted to. The corresponding second-order models are:

$$\begin{pmatrix} F_{M,myrcene} \\ F_{M,humulene} \\ F_{M,total\ mass} \end{pmatrix} = \begin{pmatrix} \boldsymbol{\beta}_{myrcene} \\ \boldsymbol{\beta}_{humulene} \\ \boldsymbol{\beta}_{total\ mass} \end{pmatrix} \bullet \begin{pmatrix} 1 \\ p \\ T \\ p^2 \\ T^2 \\ pT \end{pmatrix} = \begin{pmatrix} 2.12e08 & 4.33e05 & -1.49e06 & -329 & 2.54e03 & -1.17e03 \\ -1.81e06 & 1.35e04 & 6.05e03 & 28.7 & 2.78 & -62.9 \\ -2.00e06 & 1.39e04 & 9.35e03 & 46.6 & -5.31 & -70.9 \end{pmatrix} \bullet \begin{pmatrix} 1 \\ p \\ T \\ p^2 \\ T^2 \\ pT \end{pmatrix} \tag{35}$$

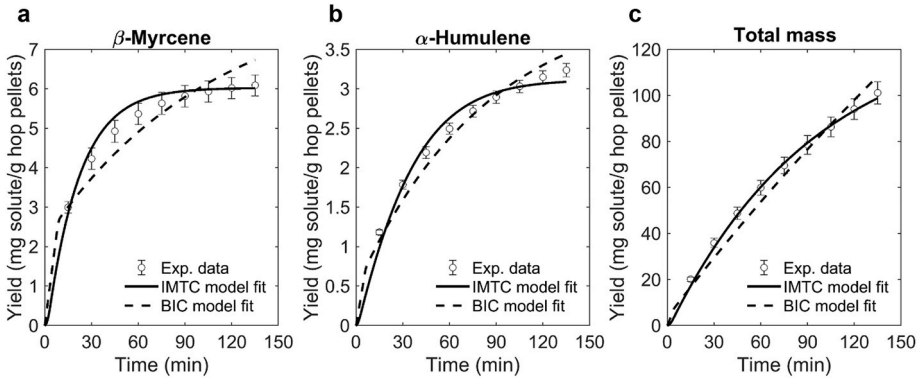

Fig. 3. Comparison of IMTC and BIC model fit for β-myrcene (a), α-humulene (b), and the total mass of extract (c) at 40 °C and 100 bar with standard deviation (duplicates).

Table 2
Model parameters of the IMTC and BIC model fitted to experimental data and respective mean absolute percentage error (MAPE) for condition T = 40 °C and p = 100 bar.

	β-Myrcene	α-Humulene	Total mass
IMTC model			
$k_i a$ (s^{-1})	8.66×10^{-4}	4.97×10^{-3}	1.25×10^{-3}
$y^*(x_0)$ (g g^{-1})	3.62×10^{-3}	3.73×10^{-4}	1.29×10^{-2}
x_0 (g g^{-1})	3.09×10^{-3}	1.60×10^{-3}	6.62×10^{-2}
MAPE (%)	3.67	4.57	3.18
AIC_c (1)	48.30	36.96	84.27
BIC model			
r (1)	0.309	0.168	0.0149
$k_s a$ (s^{-1})	5.84×10^{-5}	9.76×10^{-5}	2.06×10^{-5}
$k_f a$ (s^{-1})	0.988	0.928	0.676
$y^*(x_{1,0})$ (g g^{-1})	1.18×10^{-3}	4.37×10^{-4}	6.09×10^{-3}
MAPE (%)	6.50	5.52	8.97
AIC_c (1)	72.24	52.85	117.6

Table 3
Mean values of mean absolute percentage error (MAPE) and Akaike criterion (AIC_c) across all experimental conditions for each volatile and total mass analyzed.

	MAPE (%)		AIC_c (1)	
	IMTC	BIC	IMTC	BIC
β-Myrcene	3.72	9.10	40.42	65.17
α-Humulene	6.45	4.48	35.47	43.21
2-Methylbutyl isobutyrate	4.71	4.04	−7.07	1.51
β-Caryophyllene	6.53	4.35	13.22	19.97
Undecanone	8.15	8.86	−27.24	−14.91
Linalool	9.50	4.43	−32.63	−33.73
α-Pinene	17.56	11.15	−51.33	−47.82
Total mass	4.22	5.85	77.38	95.75

$$\begin{pmatrix} x_{0,myrcene} \\ x_{0,humulene} \\ x_{0,total\ mass} \end{pmatrix} = \begin{pmatrix} \boldsymbol{\gamma_{myrcene}} \\ \boldsymbol{\gamma_{humulene}} \\ \boldsymbol{\gamma_{total\ mass}} \end{pmatrix} \bullet \begin{pmatrix} 1 \\ p \\ T \\ p^2 \\ T^2 \\ pT \end{pmatrix} = \begin{pmatrix} -19.4 & -0.738 & 0.467 & -3.26e-03 & -1.65e-03 & 4.63e-03 \\ -138 & 0.432 & 0.739 & 1.93e-05 & -9.38e-04 & -1.37e-03 \\ -1.23e04 & -8.57 & 82.5 & -3.33e-02 & -0.143 & 5.40e-02 \end{pmatrix} \bullet \begin{pmatrix} 1 \\ p \\ T \\ p^2 \\ T^2 \\ pT \end{pmatrix} \tag{36}$$

The fitted parameters of $\boldsymbol{\beta}$ for all compounds are available in SI Table S4 online. Fig. 4 shows that the dependence of F_M on pressure and temperature differs for β-myrcene, α-humulene, and total mass. All of the other compounds exhibit a behavior similar to α-humulene, as can be seen in SI Figures S16-S20 online. An overall decrease of F_M is observed at increasing pressure and decreasing temperature for most essential oil components, a result which might be attributed to the increased co-extraction of cuticular waxes [12,46]. It has been demonstrated by Gaspar [46] that an increased extraction of cuticular waxes at higher pressures leads to a simultaneous increase in essential oil extraction. The reduction of this wax barrier contributes to a decrease in intra-particle diffusion hindrance and an increase in exposure area of essential oils. Moreover, an enhanced disruption of glandular trichomes in which the major monoterpenes and sesquiterpenes are enclosed might explain this effect [47,48]. With regard to total mass, the tendency is the opposite, which might be linked to the selection of the pseudo-solute for the D_{12} correlation in this case (weighted average of representative compounds α-humulene, isohumulone, and lupulone according to Ref. [44]) or other model simplifications [12].

Surprisingly, the fitted initial mass fraction x_0 was found to systematically change with pressure and temperature, a behavior which was unexpected and which might be attributed to unrevealed physical or chemical phenomena not covered by the model assumptions, or mutual dependence of parameters. Please note that the approaches used by the authors employing a constant value of x_0 for all p-T conditions did not yield satisfactory fitting results. The fitted function of x_0 over pressure and temperature is depicted in Fig. 5, along with the parameters of $\boldsymbol{\gamma}$ listed in SI Table S4 online. The fitted function increases at increasing pressure and decreases at increasing temperature with respect to β-myrcene and total mass. This is also the case for 2-MBIB and α-pinene (see SI Figures S22 and S25 online). In contrast, α-humulene, β-caryophyllene (SI Figure S21 online), undecanone (SI Figure S23 online), and linalool (SI Figure S24 online) exhibit a different correlation, especially at high temperatures. Basically, changes in the initial molecular mass fractions with pressure and temperature might be attributed to a change in the accessibility of essential oil due to the removal of cuticular waxes [46] (increased exposure at higher pressure), the physical integrity of glandular trichomes [47], or due to other structural changes, such as swelling [34]. It should, however, be considered that the changes of x_0 might also be a consequence of parameter fitting and hence should be interpreted with caution in the absence of experimental evidence for this behavior.

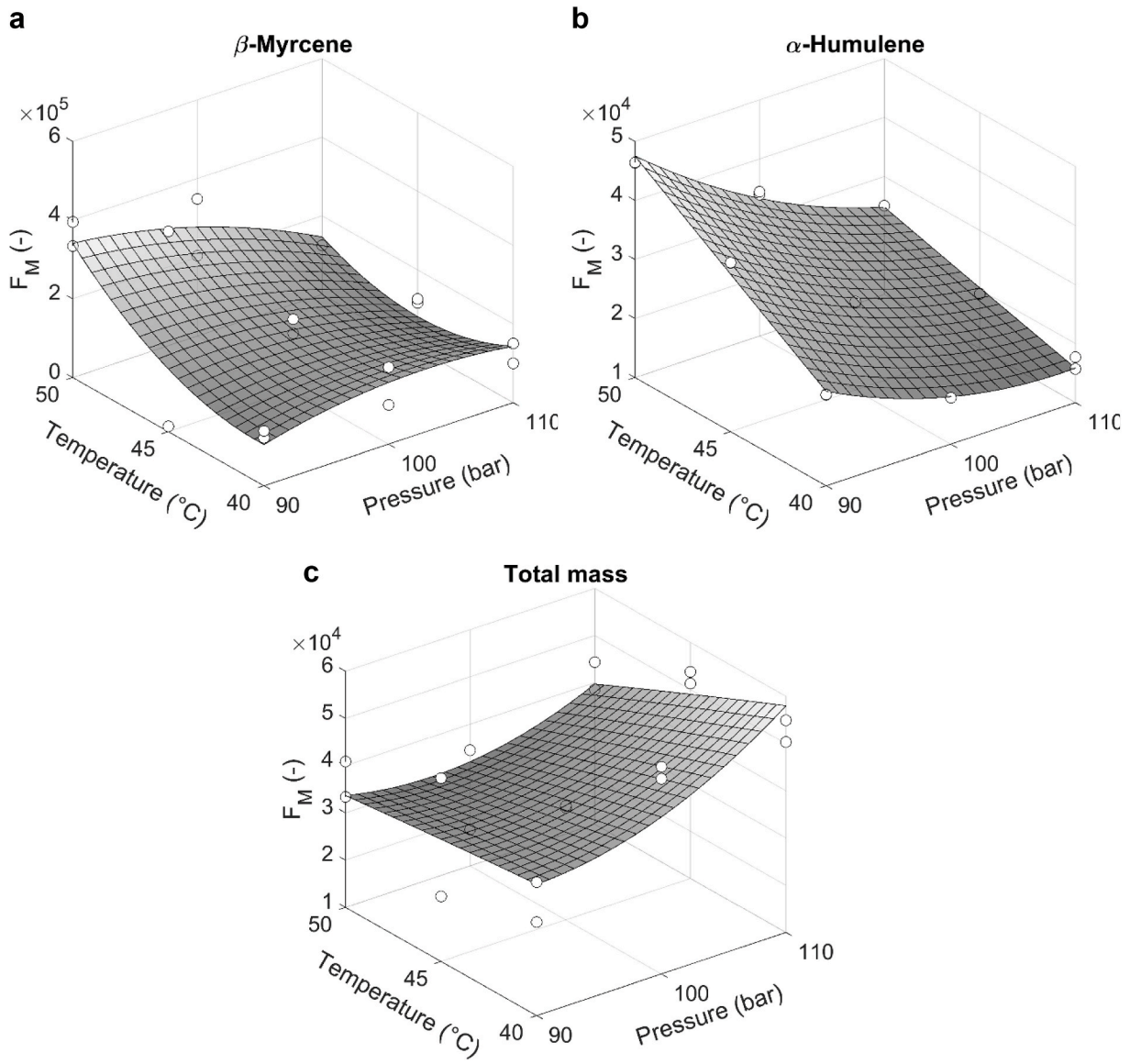

Fig. 4. Fits of microstructural factor F_M for β-myrcene (a), α-humulene (b), and the total mass of extract (c) as a function of temperature and pressure; surface plots of second-order model fitted to values of F_M obtained from fits to single experiments (◯).

Correlations of equilibrium mass fraction $y^*(x_0)$ with pressure and temperature conditions are described by the parameter vector $\boldsymbol{\alpha}$ (3 parameters; see Equations (27) and (28)). The results of $\boldsymbol{\alpha}$ are listed in Table 4 together with the MAPE average across all experiments. According to our results, the equilibrium concentrations increase with increasing pressure (α_1 positive) and decrease with increasing temperature (α_2 and α_3 negative) for all components. In other words, within the analyzed range, the lowest temperature (40 °C) and highest pressure (110 bar) were preferable for achieving the maximum essential oil yield.

This result is also evident from the extraction yield curves plotted in Figs. 6-8. Lines represent the simulated extraction kinetics of β-myrcene, α-humulene, and total mass, based on the parameterized IMTC model, whereas circles specify experimental data points (plots for other compounds available in SI Figures S26-S30 online). The highest yield is observed at 110 bar and 40 °C for most components (except linalool and undecanone; see SI Figures S11-12 online, attributed to experimental error). In a similar manner, the lowest total yield of the compounds analyzed in this research resulted from an extraction at 50 °C and 90 bar, i.e., the highest temperature and lowest pressure. Looking at yield vs. time, the highest extraction rates (slope of the curve) are always observed within the first 15 min, after which the rate of extraction decreased continuously until the end of the experiment, at 135 min. This result is in contrast to the findings by Van Opstaele et al. [20] and Langezaal et al. [49], who extracted hop oil components from hop powder and hop cones/leaves, respectively. The authors claimed that the extraction rates of some components (e.g., β-caryophyllene) can increase over time, which was not observed in our case. Comparing the sensitivity of the total extraction yield to temperature and pressure, the

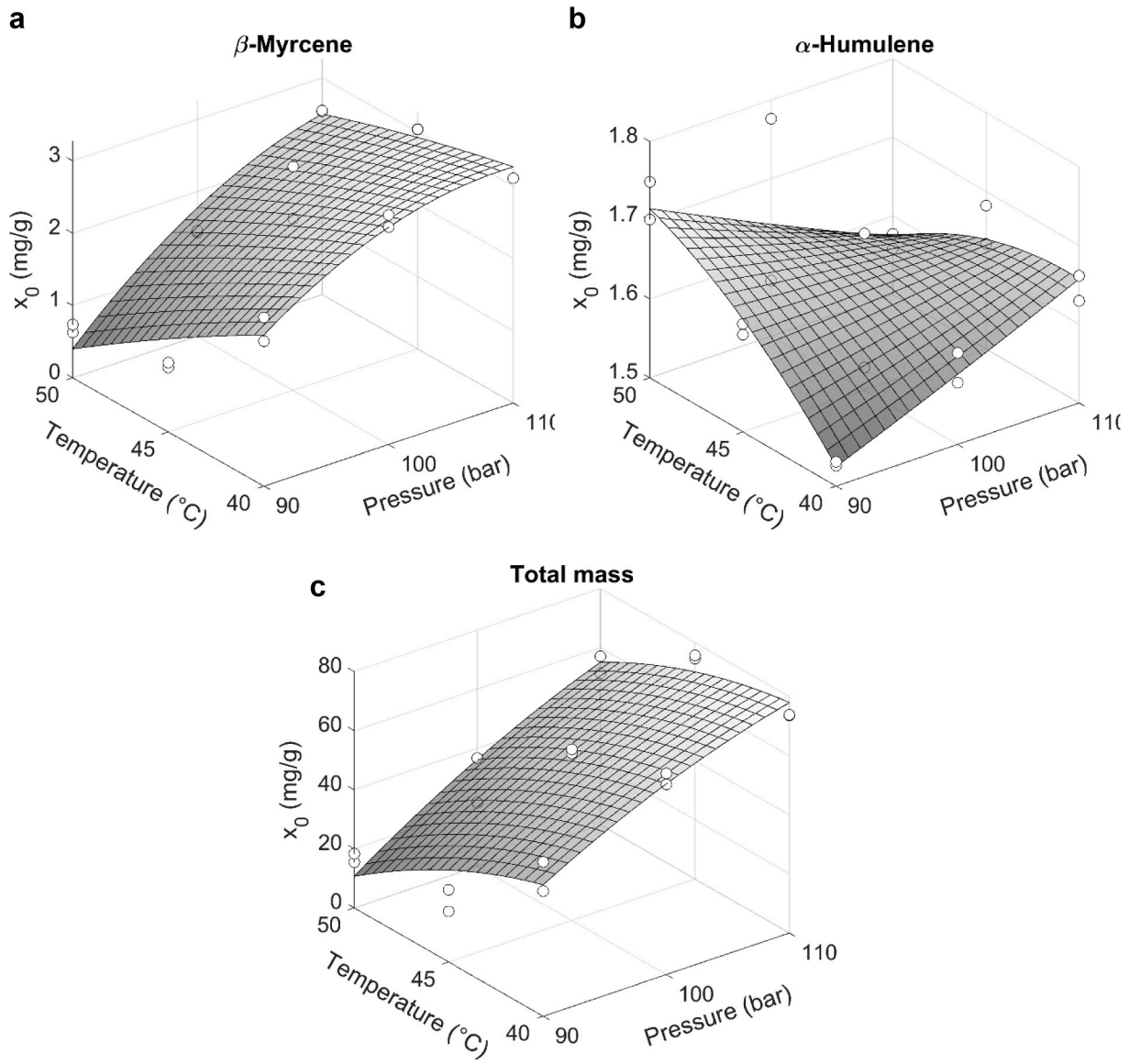

Fig. 5. Fits of initial solid-phase mass fraction x_0 for β-myrcene (a), α-humulene (b), and the total mass of extract (c) as a function of temperature and pressure; surface plots of second-order model fitted to values of x_o obtained from fits to single experiments (◯).

Table 4
Parameters of $y^*(x_0)$ as a function of temperature and pressure, fitted to all experimental data and the mean absolute percentage error (MAPE, average across all experiments).

Component	α_1	α_2	α_3	MAPE (%)
β-Myrcene	3.065	−2.638	−10.548	13.44
α-Humulene	2.822	−2.351	−12.194	8.38
β-Caryophyllene	2.789	−2.169	−13.801	8.11
2-Methylbutyl isobutyrate	2.005	−1.595	−11.218	7.29
Undecanone	2.547	−2.848	−12.746	12.40
Linalool	2.687	−0.575	−21.183	11.70
α-Pinene	2.784	−1.531	−20.034	26.75
Total mass	5.215	−2.745	−22.784	13.50

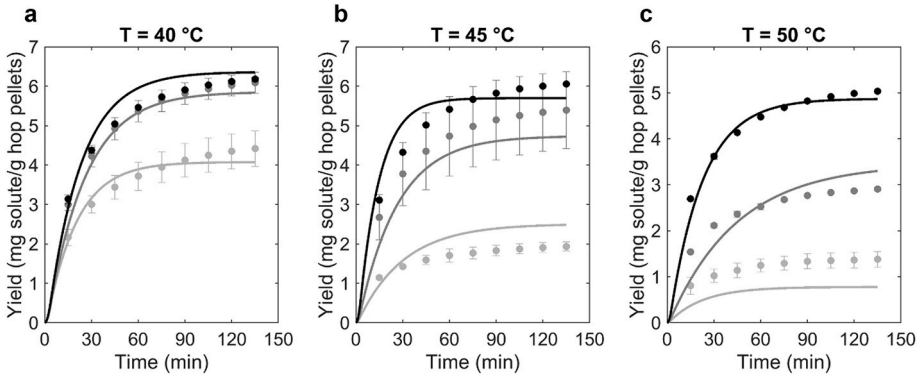

Fig. 6. Fitted extraction curves of β-myrcene (IMTC model) as functions of pressure and temperature at T = 40 °C (a), T = 45 °C (b), and T = 50 °C (c). Experimental data at p = 90 bar (●), p = 100 bar (●), and p = 110 bar (●) with standard deviation (duplicates) and IMTC model fits at p = 90 bar (−), p = 100 bar (−), and p = 110 bar (−).

effect of pressure variation is observed to be basically higher than the effect of temperature variation within the investigated range (see Figs. 6-8).

Regarding the goodness-of-fit, Table 4 shows the average MAPE values ranging between 7.29% for 2-MBIB and 26.75% for α-pinene. The results of MAPE for all individual experimental conditions are available in SI Table S5 online. For most components, the best goodness-of-fit was obtained at high pressures and low temperatures, corresponding to the highest yield. At high temperatures and low pressures, i.e., 50 °C and 90 bar, the goodness-of-fit was poor for most compounds, as was 45 °C and 90 bar, a partial explanation for which was the high standard deviation of measurements. Nevertheless, the authors are concluding that changes of $scCO_2$ extraction from hop pellets with temperature and pressure variation were able to be described appropriately for most experimental conditions and essential oil components.

The small nonpolar monoterpenes β-myrcene (Fig. 6) and α-pinene (SI Figure S30 online) extracted fastest for all tested conditions. In contrast, the large sesquiterpenes α-humulene (Fig. 7) and β-caryophyllene (SI Figure S26 online) both exhibited moderate extraction rates over the entire extraction time. This result agreed with the findings by Wei et al. [50], who investigated the SFE of α-humulene from clove oil. Molecules with intermediate molar mass (2-MBIB, undecanone, linalool), presented in SI Figures S27, S28, and S29 (available online), respectively, exhibit extraction behaviors in-between those of monoterpenes and sesquiterpenes. 2-MBIB shares similarities with the monoterpenes, undergoing a rather quick and exhaustive extraction. Linalool and undecanone are extracted more slowly. According to all these observations, extraction kinetics vary with different molecular structure and size: the smaller the molecule, the quicker it seems to be extracted.

In general, it was observed for all compounds that small variations in the operating conditions (5 °C or 10 bar) resulted in large changes in the extraction rate and essential oil composition. This result can be explained by the high compressibility of CO_2 in the pressure-temperature range under investigation, as well as the resulting variation in solvent capacity. Overall, the increase in yield at an increasing pressure and a decreasing temperature is variously pronounced for the aroma compounds. More precisely, a change in temperature, pressure, or extraction time leads to a change in the final extract composition. Comparing Figs. 6 and 7, this is particularly applicable to β-myrcene and α-humulene since the variation of yield with a change in pressure is considerably higher for β-myrcene than it is for α-humulene, i.e., pressure is expected to influence the mass ratio of these two components.

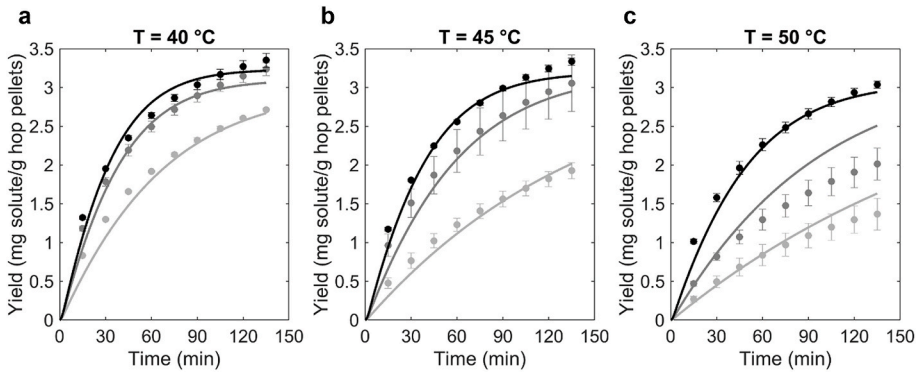

Fig. 7. Fitted extraction curves of α-humulene (IMTC model) as functions of pressure and temperature at T = 40 °C (a), T = 45 °C (b), and T = 50 °C (c). Experimental data at p = 90 bar (●), p = 100 bar (●), and p = 110 bar (●) with standard deviation (duplicates) and IMTC model fits at p = 90 bar (−), p = 100 bar (−), and p = 110 bar (−).

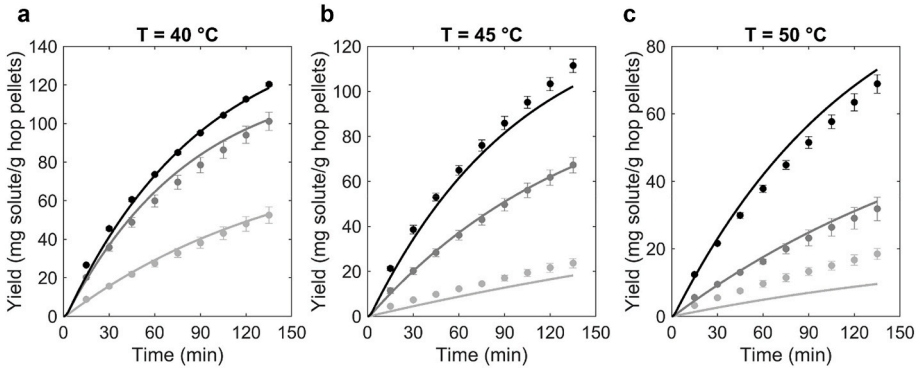

Fig. 8. Fitted extraction curves of total mass (IMTC model) as functions of pressure and temperature at T = 40 °C (a), T = 45 °C (b), and T = 50 °C (c). Experimental data at p = 90 bar (●), p = 100 bar (●), and p = 110 bar (●) with standard deviation (duplicates) and IMTC model fits at p = 90 bar (—), p = 100 bar (—), and p = 110 bar (—).

To the best of the authors' knowledge, this is the first research investigating the extraction kinetics of various different essential oil components extracted from hops and their sensitivity towards pressure and temperature. In a recent study by Nagybákay et al. (2021) [21], response surface methodology was applied to the total extract yield of SFE from hops. However, the essential oil composition of those extracts was only determined at four conditions without evaluating the kinetics of different compounds. In this study, the presented approach combines the correlation analysis of the response surface methodology regarding temperature and pressure with mechanistic modeling of extraction kinetics, and hence allows a better understanding of how aroma composition develops in the course of time.

3.3. Prediction and model validation

In order to evaluate the IMTC model prediction using the determined correlations of $k_i a(p,T)$ (based on Equations (8), (29), (30) and (35)), $y^*(p,T)$ (Equations (27) and (28)), and $x_0(p,T)$ (Equation (36)), additional extraction experiments were performed at (i) 95 bar and 48 °C, (ii) 105 bar and 42 °C, and (iii) 105 bar and 48 °C. In Fig. 9, the three simulated extraction curves are plotted together with experimental data for β-myrcene, α-humulene, and total mass. The plots for all other analyzed volatiles are available in SI Figures S31-S35 online; respective MAPE values are listed in SI Table S6 online. A good agreement of extraction kinetics is observed for α-humulene and total mass, whereas β-myrcene lacks prediction accuracy, especially at the end of extraction. An overprediction of yield after 30 min is observed for all experiments in this case. Comparing the relative deviation between predictions and experiments for all compounds, as presented in Table 5, the large sesquiterpenes α-humulene and β-caryophyllene, as well as 2-MBIB, exhibit the highest overall prediction accuracy, with a relative error between 1.5% (α-humulene at 105 bar and 42 °C and 48 °C) and 17.3% (β-caryophyllene at 95 bar and 48 °C). In contrast, the small monoterpenes β-myrcene and α-pinene are furthest from the experimental results, with a deviation of up to 44.1% (α-pinene at 105 bar and 48 °C after 30 min). One reason for this lack of predictability might have been a higher variation in the concentrations of monoterpenes. A lower overall content of β-myrcene after, in this case, approximately 5 months of storage due to chemical reactions or differences in phase partitioning could explain the overprediction in yield. The predicted qualitative changes are, however, correct for these compounds. At a high pressure and low temperature, i.e., at a higher CO_2 density, the overall error is lower for most components, which agreed with the former fitting results. From the economical perspective of an industrial user, conditions leading to higher total essential oil yields should be more attractive for application. Given that the region of interest is then the region at higher pressures, which is represented well by the IMTC model for most components and total mass (see Table 5, center and right column), we consider these limitations on accuracy to be acceptable but recommend using the model for pressures between 100 and 110 bar and temperatures between 40 and 45 °C.

Fig. 10 presents the essential oil profile of the four major oil components β-myrcene, α-humulene, β-caryophyllene, and 2-MBIB as prediction plots with different markers. The total amount of oil is approximated in this case by the sum of all seven quantified essential oil components. Values for compound content after 30 min of extraction are shown in grey, and the final content after 135 min is depicted in black. The predicted and measured contents matched well for the major components β-myrcene, α-humulene, β-caryophyllene, and 2-MBIB under all of the experimental conditions tested. Moreover, the plots highlight the differences in the extraction kinetics of monoterpenes and sesquiterpenes, and it is evident that the content of β-myrcene was much higher after 30 min than after 135 min, when the β-myrcene and α-humulene contents converged and were almost equal at 95 bar and 48 °C. This result again demonstrates that the extraction time represents another important variable to be optimized, e.g., for maximizing β-myrcene content.

Overall, the results prove that the proposed modeling approach, taking into account the parameterization for seven volatiles, is appropriate to predict the aroma composition within the experimental space of 90–110 bar and 40–50 °C. The suggested parameter fitting method applied in this scope is especially useful for components which are not freely available, e.g. due to their entrapment in glandular trichomes, and thus cannot be predicted solely by solubility models [51]. To apply the obtained results on a larger scale, it is, however, recommended to compare qualitative changes predicted by the model with large-scale experimental results, as the scope of validation is limited to the laboratory scale and the setting described in Section 2.2.1.

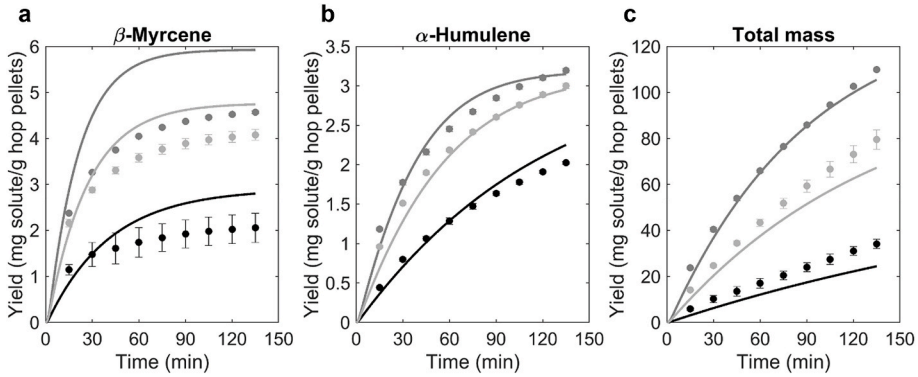

Fig. 9. IMTC model predictions of β-myrcene (a), α-humulene (b), and total mass (c) vs. experiments. Experimental data at 105 bar and 48 °C (●), 105 bar and 42 °C (●), 95 bar and 48 °C (●) with standard deviation (duplicates) and IMTC model predictions at 105 bar and 48 °C (—), 105 bar and 42 °C (—), and 95 bar and 48 °C (—).

Table 5
Relative deviation between predicted and measured extracted mass of solute after 30 min and 135 min at three different pressure and temperature conditions.

Component	Relative deviation of predicted solute mass from experiments (%)					
	95 bar and 48 °C		105 bar and 42 °C		105 bar and 48 °C	
	30 min	135 min	30 min	135 min	30 min	135 min
β-Myrcene	1.0	36.2	37.7	29.6	11.1	16.3
α-Humulene	11.3	11.2	2.9	1.5	15.0	1.5
β-Caryophyllene	3.9	17.3	5.1	4.3	9.3	3.2
2-Methylbutyl isobutyrate	9.4	6.4	15.6	9.6	3.4	1.9
Undecanone	14.9	7.1	2.9	6.6	8.6	4.0
Linalool	29.8	1.2	10.4	19.9	16.8	14.6
α-Pinene	27.4	3.8	29.2	7.4	44.1	28.7
Total mass	38.7	28.4	8.9	4.0	17.8	15.4

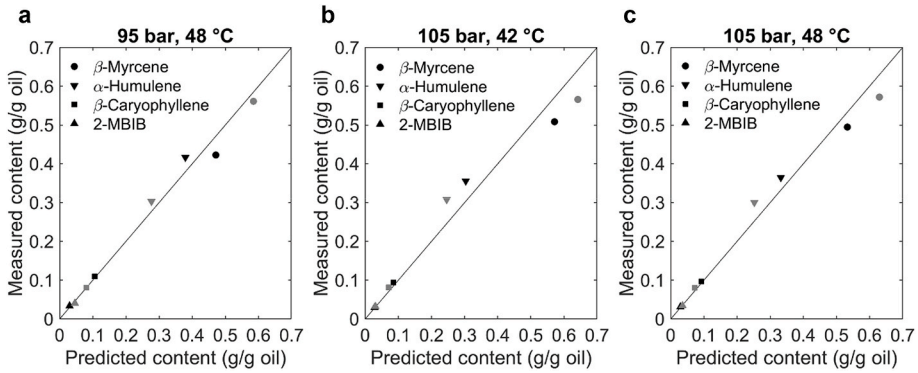

Fig. 10. Comparison of predicted and measured contents in the oil fraction of β-myrcene, α-humulene, β-caryophyllene, and 2-methylbutyl isobutyrate (2-MBIB) at 95 bar/48 °C (a), 105 bar/42 °C (b), and 105 bar/48 °C (c) after 135 min (●, ▼, ■, ▲) and 30 min (●, ▼, ■, ▲). The solid line marks zero prediction error.

4. Conclusions

The research presented herein demonstrates, through the example of hop pellet extraction using supercritical CO_2, that a combination of mechanistic modeling and fitting the model parameters as functions of temperature and pressure to experimental data enables the prediction of essential oil yield and composition. Our research found the internal-mass-transfer-control (IMTC) model [28] to be preferable over the broken-and-intact-cells model [31] (based on the modified Akaike criterion). The IMTC model was found to describe the extraction kinetics of all essential oil compounds adequately allowing the modeling of essential oil composition at different extraction times within the maximum extraction time evaluated. Three model parameters – mass transfer coefficient, initial

equilibrium concentration, and initial solid-phase concentration – were successfully described as functions of temperature and pressure by least-squares parameter fitting to the extraction kinetics of essential oil components. Unexpected changes of the solid-phase concentration with pressure and temperature were determined by parameter fitting which indicates that the physical meaning of this parameter should be interpreted with caution and might be attributed to parameter interdependence. Our results show that the yield of essential oil components increases with a rise in pressure and decreases with a rise in temperature in the range of 90–110 bar and 40–50 °C, respectively. This behavior could be described by the parameterized solubility model by Chrastil [43]. Quite different extraction kinetics and pressure sensitivities of the monoterpene β-myrcene and the sesquiterpene α-humulene highlight the fact that extract composition is adjustable through a systematic selection of processing conditions. The predictive performance of the parameterized IMTC model was shown to be excellent for sesquiterpenes, whereas the prediction of the monoterpene extraction was unsatisfactory, possibly due to evaporation when storing the material, or due to effects not considered by the model assumptions. Nonetheless, the essential oil composition was able to be predicted with a generally high level of accuracy, which represents a quick and low-cost alternative to the experimental trial-and-error strategies. Upscaling and transferability studies to other operating conditions and raw materials are beyond the scope of this article and may be investigated in future studies.

Prospectively, our findings may pave the way for process optimization with respect to temperature, pressure, and time of extraction. In order to further improve both prediction performance and generalizability, and to investigate the validity of model assumptions, additional analyses of flow and solute partitioning are recommended in the future. Potential industrial applications include the production of tailored hop aroma extracts using supercritical fluid extraction, for which model-based optimization can be applied. The aroma-intense extract can be used for the flavoring and standardization of beer in the cold stage prior to filling as an alternative to dry hopping methods. This would enable a reduction in raw material consumption and provide new products with elevated sensory quality.

Author contribution statement

Verena Bernadette Pannusch: Performed the experiments; Analyzed and interpreted the data; Contributed reagents, materials, analysis tools or data; Wrote the paper.

Lukas Viebahn: Conceived and designed the experiments; Performed the experiments; Analyzed and interpreted the data; Wrote the paper.

Heiko Briesen: Analyzed and interpreted the data.

Mirjana Minceva: Conceived and designed the experiments; Analyzed and interpreted the data; Contributed reagents, materials, analysis tools or data.

Funding statement

This research did not receive any specific grant from funding agencies in the public, commercial, or not-for-profit sectors.

Data availability statement

Data will be made available on request.

Declaration of interest's statement

The authors declare no competing interests.

Acknowledgements

The authors would like to thank Dr. Martin Biendl and the Simon H. Steiner, Hopfen, GmbH for kindly supplying the hop samples. We would also like to express our special thanks to Dr. Simon Vlad Luca and Friederike Deckwerth for their valuable advice and support.

Appendix A. Solid density and porosity

The solid density ρ_s measured by helium pycnometry before extraction was 1312 kg m^{-3} ± 2 kg m^{-3} and 1316 kg m^{-3} ± 10 kg m^{-3} after 135 min of extraction at 90 bar and 45 °C. Given that the change of density throughout extraction proved to be within the standard deviation, the solid density value after extraction was used as a parameter for the simulations of extraction kinetics and assumed to be constant throughout extraction. The total porosity ε, calculated according to Equation (4) was found to be 0.49 before and 0.50 after 135 min of extraction at 90 bar and 45 °C. Due to this very small change, a constant porosity of $\varepsilon = 0.50$ was defined for simulations.

Appendix B. Supplementary data

Supplementary data related to this article can be found at https://doi.org/10.1016/j.heliyon.2023.e13030.

References

[1] M. Herrero, et al., Supercritical fluid extraction: recent advances and applications, J. Chromatogr. A 1217 (16) (2010) 2495–2511.
[2] V. Illés, et al., Extraction of coriander seed oil by CO_2 and propane at super-and subcritical conditions, J. Supercrit. Fluids 17 (2) (2000) 177–186.
[3] D.G. Wilson, Plant remains from the Graveney boat and the early history of *Humulus lupulus* L. in W. Europe, New Phytol. 75 (3) (1975) 627–648.
[4] K. Goiris, et al., The flavoring potential of hop polyphenols in beer, J. Am. Soc. Brew. Chem. 72 (2) (2014) 135–142.
[5] W.J. Simpson, P.S. Hughes, Stabilization of Foams by Hop-Derived Bitter Acids. Chemical Interactions in Beer Foam, Cerevisia and Biotechnology, Belgium), 1994.
[6] C. Almaguer, et al., Humulus lupulus - a story that begs to be told. A review, J. Inst. Brew. 120 (4) (2014) 289–314.
[7] N. Rettberg, M. Biendl, L.-A. Garbe, Hop aroma and hoppy beer flavor: chemical backgrounds and analytical tools - a review, J. Am. Soc. Brew. Chem. 76 (1) (2018) 1–20.
[8] F. Sharpe, D. Laws, The essential oil of hops a review, J. Inst. Brew. 87 (2) (1981) 96–107.
[9] M. Biendl, et al., 1, Fachverlag Hans Carl. (2015) 53–54.
[10] Y. Liu, et al., Antioxidant activities of hops (*Humulus lupulus*) and their products, J. Am. Soc. Brew. Chem. 65 (2) (2007) 116–121.
[11] T. Fornari, et al., Isolation of essential oil from different plants and herbs by supercritical fluid extraction, J. Chromatogr. A 1250 (2012) 34–48.
[12] K. Araus, E. Uquiche, J.M. del Valle, Matrix effects in supercritical CO_2 extraction of essential oils from plant material, J. Food Eng. 92 (4) (2009) 438–447.
[13] S.M. Pourmortazavi, S.S. Hajimirsadeghi, Supercritical fluid extraction in plant essential and volatile oil analysis, J. Chromatogr. A 1163 (1–2) (2007) 2–24.
[14] M.M.R. de Melo, A.J.D. Silvestre, C.M. Silva, Supercritical fluid extraction of vegetable matrices: applications, trends and future perspectives of a convincing green technology, J. Supercrit. Fluids 92 (2014) 115–176.
[15] L. Baldino, R. Adami, E. Reverchon, Concentration of Ruta graveolens active compounds using SC-CO_2 extraction coupled with fractional separation, J. Supercrit. Fluids 131 (2018) 82–86.
[16] L.C. dos Santos, et al., Integrated supercritical CO_2 extraction and fractionation of passion fruit (Passiflora edulis Sims) by-products, J. Supercrit. Fluids (2021) 168.
[17] A. Forster, et al., Advances in hop extraction with supercritical carbon dioxide, Brauwelt Int. 5 (2020) 324–330.
[18] D. De Kjujkeleire, et al., Automated reporting on the quality of hops and hop products, J. Inst. Brew. 104 (2) (1998) 75–82.
[19] M. Verschuere, P. Sandra, F. David, Fractionation by SFE and microcolumn analysis of the essential oil and the bitter principles of hops, J. Chromatogr. Sci. 30 (10) (1992) 388–391.
[20] F. Van Opstaele, et al., Production of novel varietal hop aromas by supercritical fluid extraction of hop pellets - Part 2: preparation of single variety floral, citrus, and spicy hop oil essences by density programmed supercritical fluid extraction, J. Supercrit. Fluids 71 (2012) 147–161.
[21] N.E. Nagybákay, et al., Optimized supercritical CO_2 extraction enhances the recovery of valuable lipophilic antioxidants and other constituents from dual-purpose hop (*Humulus lupulus* L.) variety ella, Antioxidants 10 (918) (2021).
[22] K. Bizaj, et al., Sub-and supercritical extraction of slovenian hops (Humulus lupulus L.) aurora variety using different solvents, Plants 10 (6) (2021) 1137.
[23] S.C. Kupski, et al., Mathematical modeling of supercritical CO_2 extraction of hops (*Humulus lupulus* L.), J. Supercrit. Fluids 130 (2017) 347–356.
[24] H. Sovová, Rate of the vegetable oil extraction with supercritical CO_2 - I. Modelling of extraction curves, Chem. Eng. Sci. 49 (3) (1994) 409–414.
[25] E.M.C. Reis-Vasco, et al., Mathematical modelling and simulation of pennyroyal essential oil supercritical extraction, Chem. Eng. Sci. 55 (15) (2000) 2917–2922.
[26] M.R. García-Risco, et al., Kinetic study of pilot-scale supercritical CO_2 extraction of rosemary (Rosmarinus officinalis) leaves, J. Supercrit. Fluids 55 (3) (2011) 971–976.
[27] P.M. Moura, et al., Supercritical fluid extraction from guava (Psidium guajava) leaves: global yield, composition and kinetic data, J. Supercrit. Fluids 62 (2012) 116–122.
[28] J.M. del Valle, P. Napolitano, N. Fuentes, Estimation of relevant mass transfer parameters for the extraction of packed substrate beds using supercritical fluids, Ind. Eng. Chem. Res. 39 (12) (2000) 4720–4728.
[29] K. Verschueren, Dry hopping process challenges, Brauwelt Int. 2 (2019) 127–129.
[30] D. Saison, et al., Optimisation of a complete method for the analysis of volatiles involved in the flavour stability of beer by solid-phase microextraction in combination with gas chromatography and mass spectrometry, J. Chromatogr. A 1190 (1–2) (2008) 342–349.
[31] H. Sovová, Mathematical model for supercritical fluid extraction of natural products and extraction curve evaluation, J. Supercrit. Fluids 33 (1) (2005) 35–52.
[32] E. Reverchon, C. Marrone, Supercritical extraction of clove bud essential oil: isolation and mathematical modeling, Chem. Eng. Sci. 52 (20) (1997) 3421–3428.
[33] E. Reverchon, Mathematical modeling of supercritical extraction of sage oil, AIChE J. 42 (6) (1996) 1765–1771.
[34] M. Stamenic, et al., Swelling of plant material in supercritical carbon dioxide, J. Supercrit. Fluids 52 (1) (2010) 125–133.
[35] A. Berna, A. Cháfer, J.B. Montón, Solubilities of essential oil components of orange in supercritical carbon dioxide, J. Chem. Eng. Data 45 (5) (2000) 724–727.
[36] J. da Cruz Francisco, B. Sivik, Solubility of three monoterpenes, their mixtures and eucalyptus leaf oils in dense carbon dioxide, J. Supercrit. Fluids 23 (1) (2002) 11–19.
[37] W.G. Bickley, Formulae for numerical differentiation, Math. Gaz. 25 (263) (2016) 19–27.
[38] J. Puiggené, M.A. Larrayoz, F. Recasens, Free liquid-to-supercritical fluid mass transfer in packed beds, Chem. Eng. Sci. 52 (2) (1997) 195–212.
[39] O.J. Catchpole, M.B. King, Measurement and correlation of binary diffusion coefficients in near critical fluids, Ind. Eng. Chem. Res. 33 (7) (1994) 1828–1837.
[40] R. Span, W. Wagner, A new equation of state for carbon dioxide covering the fluid region from the triple-point temperature to 1100 K at pressures up to 800 MPa, J. Phys. Chem. Ref. Data 25 (6) (1996) 1509–1596.
[41] A. Laesecke, C.D. Muzny, Reference correlation for the viscosity of carbon dioxide, J. Phys. Chem. Ref. Data 46 (1) (2017).
[42] M.R.E. Symonds, A. Moussalli, A brief guide to model selection, multimodel inference and model averaging in behavioural ecology using Akaike's information criterion, Behav. Ecol. Sociobiol. 65 (1) (2010) 13–21.
[43] J. Chrastil, Solubility of solids and liquids in supercritical gases, J. Phys. Chem. 86 (15) (1982) 3016–3021.
[44] J.M. del Valle, et al., *Mass transfer and equilibrium parameters on high-pressure CO_2 extraction of plant essential oils*, in: Food Engineering Interfaces, Springer, 2010, pp. 393–470.
[45] A. Formato, et al., Supercritical fluid extraction of α-and β-acids from hops compared to cyclically pressurized solid–liquid extraction, J. Supercrit. Fluids 84 (2013) 113–120.
[46] F. Gaspar, *Extraction of essential oils and cuticular waxes with compressed CO_2: Effect of extraction pressure and temperature*, Ind. Eng. Chem. Res. 41 (10) (2002) 2497–2503.
[47] F. Gaspar, R. Santos, M.B. King, Disruption of glandular trichomes with compressed CO_2: alternative matrix pre-treatment for CO_2 extraction of essential oils, J. Supercrit. Fluids 21 (1) (2001) 11–22.
[48] G. Wang, et al., Terpene biosynthesis in glandular trichomes of hop, Plant Physiol. 148 (3) (2008) 1254–1266.
[49] C.R. Langezaal, et al., Analysis of supercritical carbon dioxide extracts from cones and leaves of a *Humulus lupulus* L cultivar, J. Sci. Food Agric. 53 (4) (1990) 455–463.
[50] M.-C. Wei, J. Xiao, Y.-C. Yang, Extraction of a-humulene-enriched oil from clove using ultrasound-assisted supercritical carbon dioxide extraction and studies of its fictitious solubility, Food Chem. 210 (2016) 172–181.
[51] L.M. Valenzuela, A.G. Reveco-Chilla, J.M. del Valle, Modeling solubility in supercritical carbon dioxide using quantitative structure–property relationships, J. Supercrit. Fluids 94 (2014) 113–122.